Thermal dissipation as both the strength and weakness of matter. A material failure prediction by monitoring creep

Electronic Supplementary Information (ESI)

Tom Vincent-Dospital,[1,2,*] Renaud Toussaint,[1,2,†] Alain Cochard,[1] Eirik G. Flekkøy,[2] and Knut Jørgen Måløy[2]

[1] *Université de Strasbourg, CNRS, ITES UMR 7063, Strasbourg F-67084, France*
[2] *SFF Porelab, The Njord Centre, Department of physics, University of Oslo, Norway*

CONTENTS

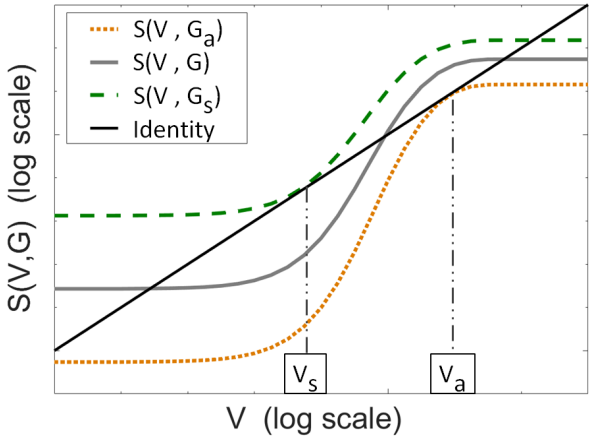

FIG. 1. Representation of $V = S(V, G)$ for three values of G: G_s, G_a and a mid-value between G_s and G_a (plain plot). The intersections of S_G with the identity plot (straight line) give the possible crack velocities for a given energy release rate, as per Eq. (4). The axes are not annotated for the sake of generality. See Ref. [2] for further information.

I. ANALYTICAL APPROXIMATION OF THE AVALANCHE THRESHOLD

Let us start this additional material with the analytical approximations of the temperature at a running crack tip. Assuming a quasi-constant velocity and energy release rate, some simplified expressions can indeed be derived[1] for ΔT. At low velocity, the typical diffusion skin depth is large compared to the radius of the heat production zone ($\sqrt{\lambda l/(V\pi C)}/l \gg 1$) and the heat diffusion is hence the ruling process:

$$\Delta T_{\text{slow}} \sim \phi G \frac{V}{\lambda}. \tag{1}$$

At high velocity, however, the rise in temperature is limited by the scale over which heat is produced and:

$$\Delta T_{\text{fast}} \sim \frac{\phi G}{\pi C l}. \tag{2}$$

Between these two cases, and typically for $V \sim \lambda/(\pi C l)$, an intermediate regime holds:

$$\Delta T_{\text{mid}} \sim \phi G \sqrt{\frac{V}{4\pi C \lambda l}}. \tag{3}$$

We invite the reader to a more in-depth derivation of these equations in Toussaint et al.[1] or Vincent-Dospital et al.[2].

Now that some straightforward expressions for ΔT are known, we can move on to infer G_a. Our model, the Arrhenius law as considered in the main manuscript, defines a function $S(V, G)$ such that $S(V, G) = V$:

$$S(V,G) = V_0 \min\left[\exp\left(-\frac{\alpha^2[G_c - G]}{k_B[T_0 + \Delta T(V,G)]}\right), 1\right]. \tag{4}$$

To lighten the equations that will follow, we have here denoted α^2 the ratio $d_0^3/(2l)$. We have discussed, in the main manuscript, how this relation might have one to three solutions depending on G (see Fig. 1). Two particular energy release rates mark the passages from a singular to multiple solutions: the avalanche threshold G_a, of interest in this study, and another threshold, G_s, which is the load at which an avalanche has to stop.
All functions being continuously smooth, the switch from one solution to three solutions implies that $S(V, G)$ is tangent to the identity function for these two particular G, as illustrated in Fig 1. G_a and the corresponding velocity V_a must therefore verify the following system of equations:

* tom.vincent-dospital@fys.uio.no
† renaud.toussaint@unistra.fr

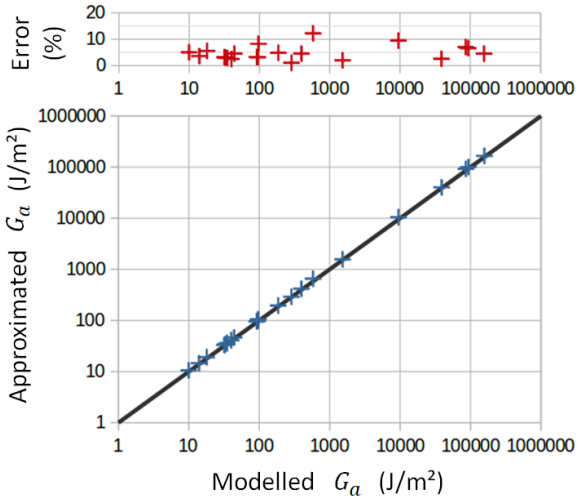

FIG. 2. (Bottom): G_a threshold, as approximated by Eq. (11) versus the accurate numerical solution of the model. The black line is the identity. (Top): Relative error from the approximation

$$S(V,G) = V \tag{5}$$

$$\frac{\partial S}{\partial V}(V,G) = 1. \tag{6}$$

To solve this system, we assume that the transition towards the fast phase happens in a regime where the temperature elevation still increases linearly with the crack velocity (i.e., $\Delta T = \Delta T_{\rm slow}(V,G)$ (1)). Equation (6) then becomes:

$$\frac{\phi G \lambda \alpha^2 (G_c - G)}{k_b(\lambda T_0 + \phi G V)^2} S(V,G) = 1. \tag{7}$$

Inserting Eq. (5) back into (7) leads to the following quadratic equation in V:

$$\left(\frac{\phi G V}{\lambda T_0}\right)^2 + \left[2 + \frac{\alpha^2(G-G_c)}{k_b T_0}\right]\frac{\phi G V}{\lambda T_0} + 1 = 0. \tag{8}$$

While it might of course hold two solutions, only the lower one is of interest to derive the avalanche threshold G_a. The upper solution would indeed correspond to the 'arrest' of the crack avalanche, but the initial hypothesis of $\Delta T = \Delta T_{\rm slow}$ would there be wrong anyway, as this 'arrest' occurs while on the quick (hot) propagation branch. Focusing therefore on the lower solution of (8), we have:

$$V_a = \frac{T_0 \lambda}{2\phi G_a}(R_a - 2 - R_a\sqrt{1 - 4/R_a}), \tag{9}$$

with $R_a = \alpha^2(G_c - G_a)/(k_B T_0)$. This equation indicates at which slow velocity a crack avalanches, given the corresponding G_a threshold. Substituting (9) in (5), one finally derives the equality that defines the avalanche threshold:

$$G_a \sim \frac{\lambda T_0}{2\phi V_0} \frac{R_a - 2 - R_a\sqrt{1 - 4/R_a}}{\exp\left(-2/\left[1 - \sqrt{1 - 4/R_a}\right]\right)}. \tag{10}$$

Such an expression gives a fairly good approximation of G_a as predicted by the model. The only hypothesis was indeed the validity of Eq. (1), that is $\sqrt{\lambda l/(V_a \pi C)}/l \gg 1$ and, for the materials that we have studied in our manuscript, this ratio ranges from 300 to 1500. While Eq. (10) is easy to solve for G_a with any numerical method, it can however be further simplified by grossly assuming that $R_a \gg 4$ and by developing the term $\sqrt{1 - 4/R_a}$. We thus obtain the equation presented in the manuscript:

$$G_a \sim \frac{\lambda T_0}{\phi V_0} \frac{\exp(R_a)}{R_a}. \tag{11}$$

Figure 2 shows the quality of the approximation for G_a, off by a few percents as, as shown in Tab. I, the $R_a \gg 4$ hypothesis is not strictly valid.

II. THE ARREST THRESHOLD (FOR COMPLETENESS)

Similarly, one can solve (5) and (6) at the 'arrest' point: the transition from a quick regime back to the low velocity phase, occurring at the particular load G_s. While G_a is vastly reported for a lot of materials, making it the topic of this manuscript, G_s is more rarely reported, so that the following computation is given for completeness. We here assume that the transition arises when the crack cools down from the plateau temperature $\Delta T = \Delta T_{\rm fast}(G)$ (2), along the intermediate slope defined by $\partial \Delta T/\partial V = \partial \Delta T_{\rm mid}(V,G))/\partial V$ (3). We thus turn the system into a quadratic equation of $\sqrt{V}$:

$$\left(\frac{\phi G\sqrt{V}}{4\pi\lambda C l T_0}\right)^2 + \left(2 + \frac{\alpha^2(G-G_c)}{2k_b T_0}\right)\left(\frac{\phi G\sqrt{V}}{4\pi\lambda C l T_0}\right) + 1 = 0, \tag{12}$$

the upper solution of which, together with Eq. (5), leads to:

$$V_s = \frac{\pi\lambda C l {T_0}^2}{4(\phi G_s)^2}\left[R_s - 4 + R_s\sqrt{1 - 8/R_s}\right]^2, \tag{13}$$

where $R_s = \alpha^2(G_c - G_s)/(k_B T_0)$. When inserting (13) back into (5), one gets:

$$\frac{4(\phi G_s)^2 V_0}{\pi\lambda C l {T_0}^2} = \frac{\left[R_s - 4 + R_s\sqrt{1-8/R_s}\right]^2}{\exp\left(\dfrac{\alpha^2(G_s - G_c)}{k_b[T_0 + \phi G_s/(\pi C l)]}\right)}. \qquad (14)$$

Assuming that $R_s \gg 8$ and $\Delta T_{\text{fast}} \gg T_0$, Eq. (14) further simplifies to:

$$G_s \sim \frac{T_0}{\phi}\sqrt{\frac{\pi\lambda C l}{V_0}}\exp\left(\frac{\pi C l T_0}{2\phi G_s}\right) R_s, \qquad (15)$$

which gives a relatively simple expression to invert for G_s.

III. SENSITIVITY OF THE ϕ PARAMETER

The percentage ϕ of energy that is converted into heat in the heat zone of radius l is a parameter that we have broadly assumed to be 0.5. In practice, this parameter is unknown, and shall likely be material dependent. In Fig. 3, we show the variation in our model prediction of the failure threshold G_a when varying ϕ, for three materials spanning the whole range of considered toughnesses. The higher ϕ, the less is G_a (e.g., see Eq.(11)), as it makes the crack tip hotter at a lower load. As shown in the figure, when considering small values of this heat efficiency, one can also obtain an all ductile behavior [2], as the crack becomes too cold to hold an instability in its dynamics. In this case, the modelled crack velocity only increases exponentially to V_0, as a function of the energy release rate G, and no velocity jump (defining G_a) is obtained.

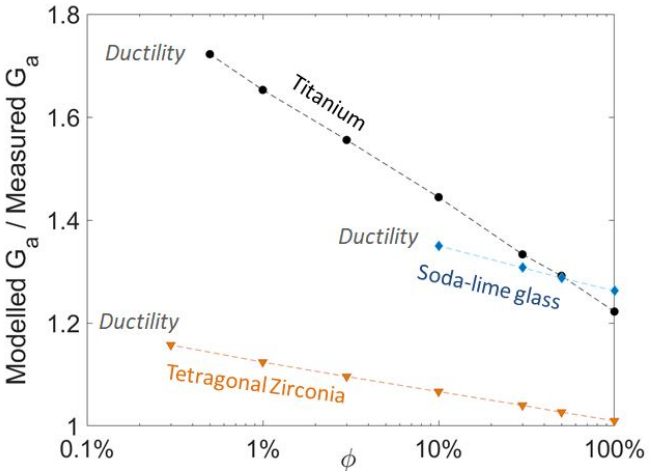

FIG. 3. Variation of the model predicted failure threshold G_a as a function of the heat efficiency ϕ, relative to the experimentally reported G_a, for a Titanium alloy ($G_c \sim 190\,\text{kJ m}^{-2}$), TZP ceramic ($G_c \sim 1900\,\text{J m}^{-2}$), and soda-lime glass ($G_c \sim 12\,\text{J m}^{-2}$). The considered model parameters for these materials are shown in table I.

IV. MATERIALS CREEP CROSSPLOTS AND PARAMETERS TABLE

A summary of the model parameters considered for each media is also provided in Tab. I. These parameters are deduced, as explained in the main manuscript, from the V to G creep data of these materials, shown in Fig 4 to Fig 21. One can notably notice the variability in fit quality for these datasets, that of course impacts our inversion work, but also how it is not always straightforward to know to which subcritical phase the data correspond (i.e., phase I to III, from environmental induced corrosion to void-like conditions).

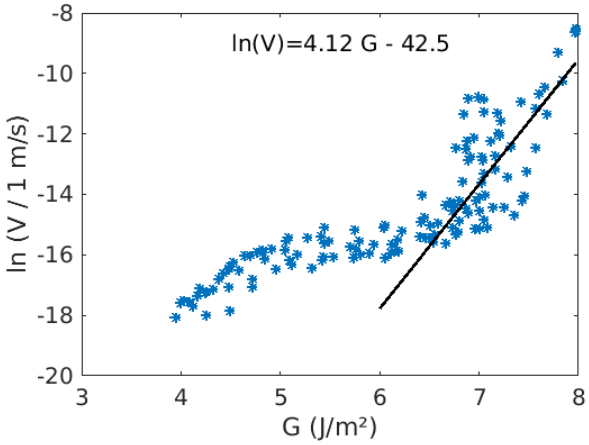

FIG. 4. Creep data of dry soda-lime glass, from Wiederhorn [3], figure 3. A rather complex creep law holds there so that we only roughly fitted the last part (i.e., stage III).

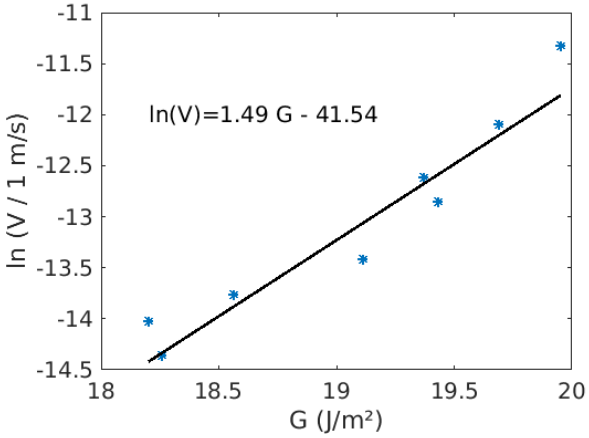

FIG. 5. Creep data of dry sapphire (r-plane), from Wiederhorn and Krause [4].

	λ (SI)	ϕ (-)	V_0 (m/s)	l (Å)	T_0 (K)	G_c (J/m^2)	G_a real (J/m^2)	G_a model (J/m^2)	Ra (-)
Acrylic adhesive	0.4	1	30	10	296	**150**	**90**	**97**	5.7
Paper	0.035	0.12	1300	1000	296	**25000**	**14000**	**9500**	15.6
Bulk PMMA	0.18	0.2	880	80	296	**1300**	**700**	**580**	10.9
Interfacial PMMA	0.18	0.2	880	8	298	**275**	**140**	**190**	13.5
HD Polyethylene	0.4	0.5	900	8500	293	**200000**	**70000**	**87000**	16.6
Soda lime glass	1	0.5	3400	0.3	296	**12**	**8**	**10**	8.3
Sapphire	24	0.5	6000	0.8	296	**36**	**20**	**32**	6
Quartz	8	0.5	3400	0.6	293	**21**	**13**	**18**	5.7
Westerly Granite (ambient)	2	0.5	3000	4	293	**120**	**68**	**92**	8.5
Westerly Granite (hot)	2	0.5	3000	0.7	573	**43**	**24**	**35**	6.8
Kumamoto Andesite	1	0.5	2200	3	330	**120**	**80**	**97**	8.8
Scioto Sandstone	2	0.5	2000	2	296	**55**	**37**	**44**	7.3
Cement paste	1	0.5	2200	3	298	**310**	**250**	**280**	10.7
HSULP Concrete	0.8	0.5	3000	1	293	**44**	**38**	**40**	9.9
Vitreous carbon	5	0.5	2600	0.2	296	**15**	**13**	**14**	7.2
Lead Zirconate Titanate (PZT)	1	0.5	2000	1	296	**40**	**24**	**33**	11.3
Tetragonal zirconia (TZP)	2	0.5	1600	40	298	**1900**	**1500**	**1530**	10.9
Silicon nitride	30	0.5	5500	45	1573	**510**	**260**	**400**	8.9
2650 T6 Aluminium alloy	150	0.5	3100	1000	448	**54500**	**27000**	**39000**	10.1
AISI 310S Stainless Steel alloy	14	0.5	3000	9000	298	**265000**	**102000**	**158000**	13.4
Ti-6A1-6V-2Sn Titanium	7	0.5	3100	8000	298	**190000**	**72000**	**93000**	14.9

TABLE I. Model parameters for various materials of the literature. The real and modelled G_a thresholds are compared in the two former last columns. The cells colour help to highlight standing out values for λ and T_0.

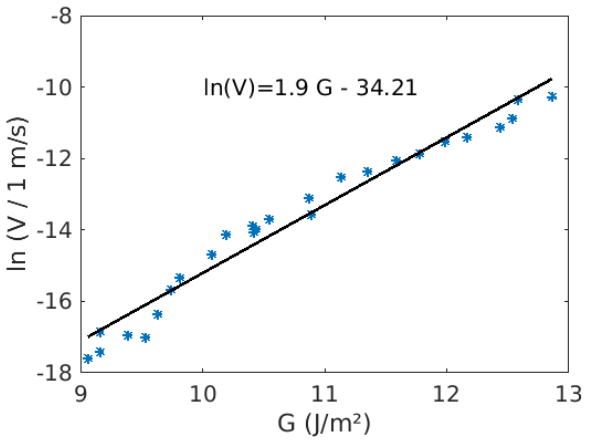

FIG. 6. Creep data of quartz in vacuum, from Dove[5], figure 4.

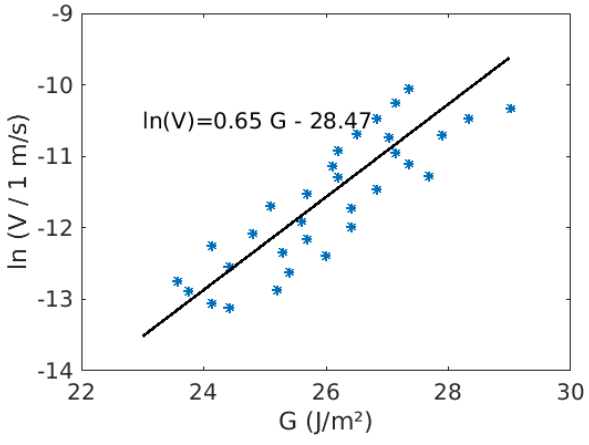

FIG. 7. Creep data of Scioto sandstone, from Holder et al.[6], figure 3.

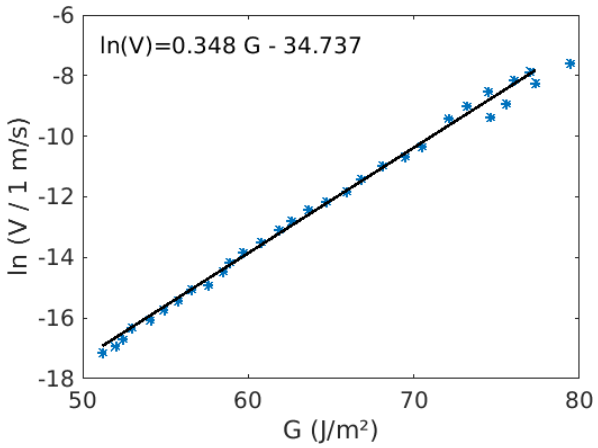

FIG. 8. Creep data of Kumamoto andesite in moist air at 67 °C, from Nara and Kaneko[7], figure 9.

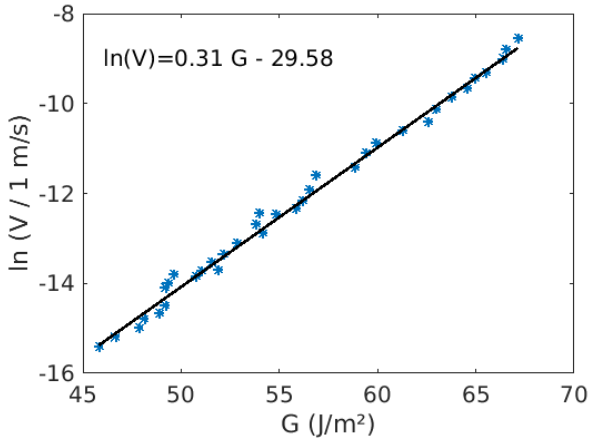

FIG. 9. Creep data of Westerly granite in moist air at 20 °C, from Meredith and Atkinson[8], figure 7.

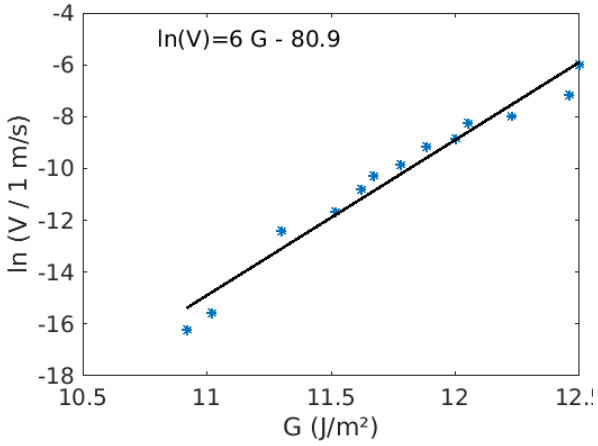

FIG. 10. Creep data of vitreous carbon, from Nadeau[9], figure 4.

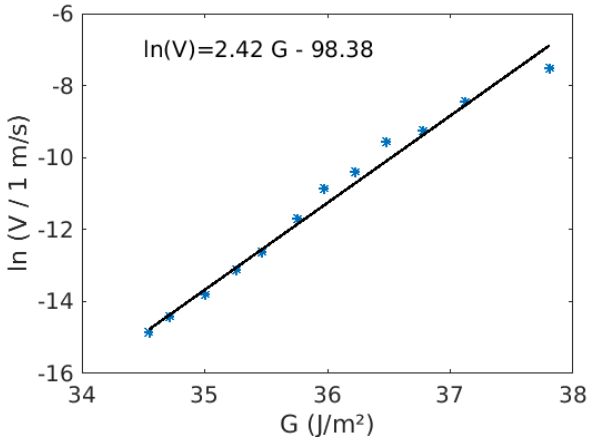

FIG. 11. Creep data of high strength ultra low porosity concrete in moist air, from Nara et al.[10], figure 9.

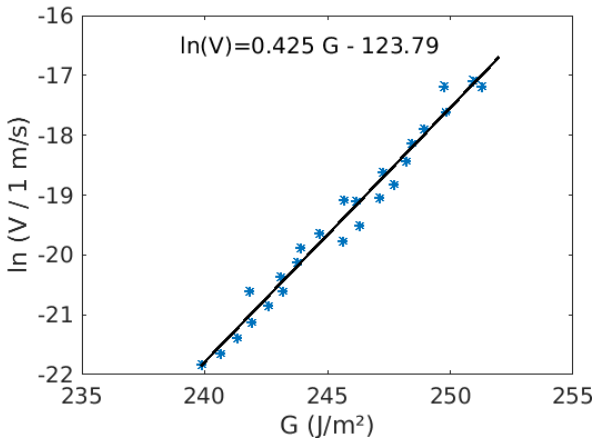

FIG. 12. Creep data cement in water, from Wang et al.[11], figure 4a.

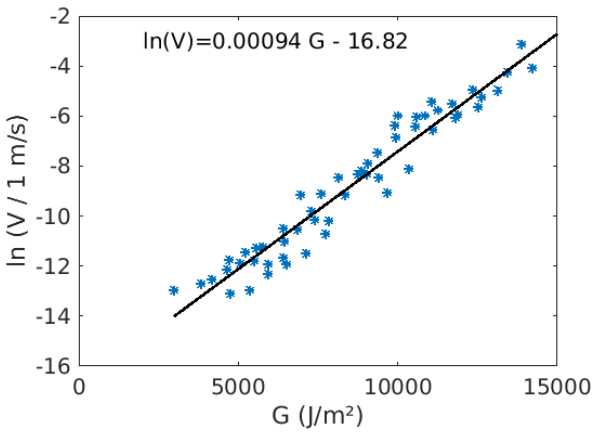

FIG. 13. Creep data of paper in air, from Santucci[12], figure 3.32.

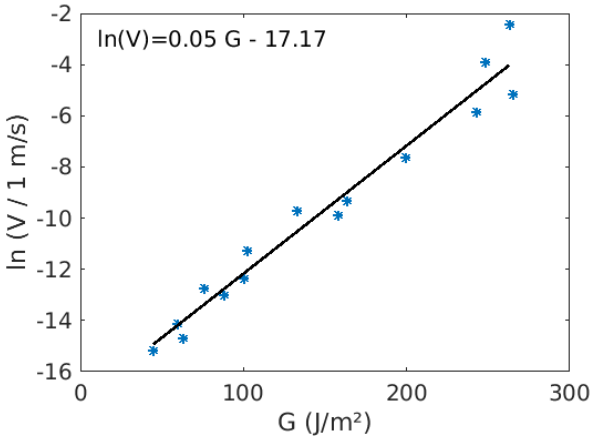

FIG. 14. Creep data of hot silicon nitride at 1200 °C, from Evans and Wiederhorn[13], figure 5.

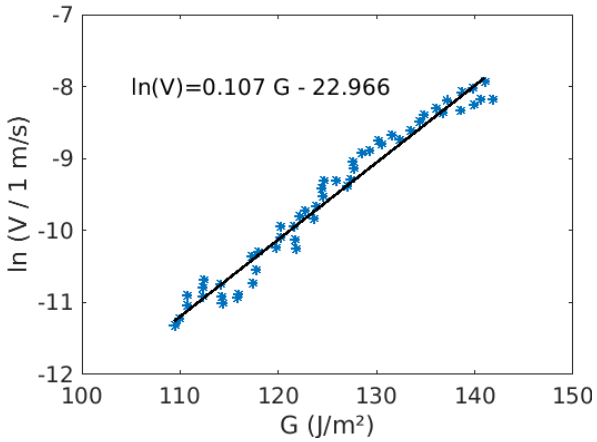

FIG. 17. Interfacial creep data in sintered PMMA plates in air, from Lengliné et al.[16], figure 5.

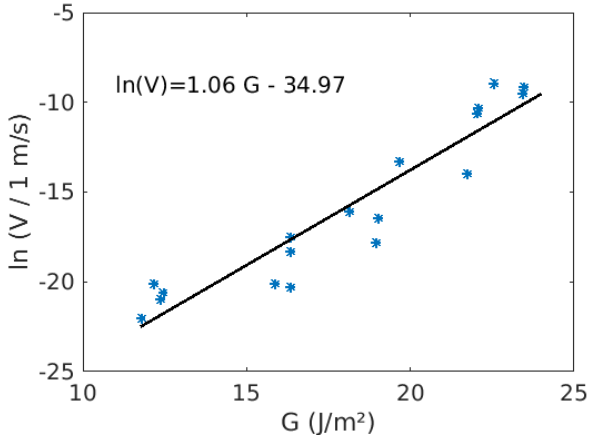

FIG. 15. Creep data of Lead Zirconate Titanate at ambient conditions, from Oates et al.[14], figure 2 (open circuit).

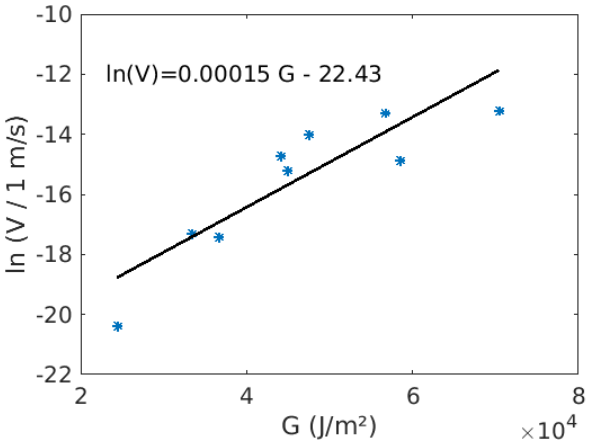

FIG. 18. Creep data of high density polyethylene, from Yoda et al.[17], figure 4.

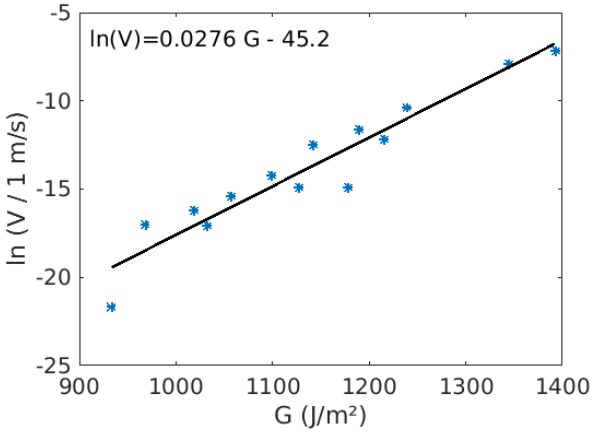

FIG. 16. Creep data tetragonal zirconia (TZP) in vacuum, from Chevalier et al.[15], figure 5.

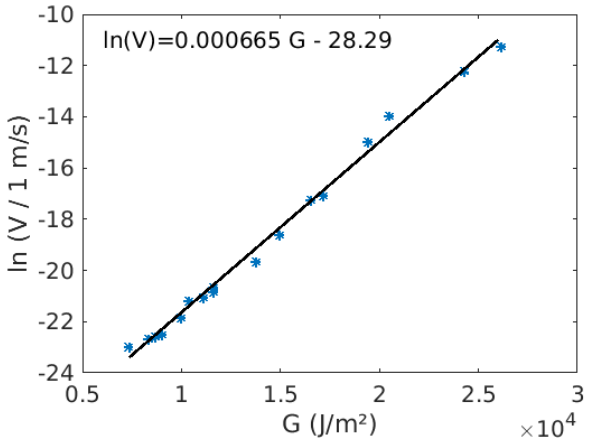

FIG. 19. Creep data of aluminium 2650 T6 alloy in vacuum at 175 °C, from Hénaff et al.[18], figure 6.

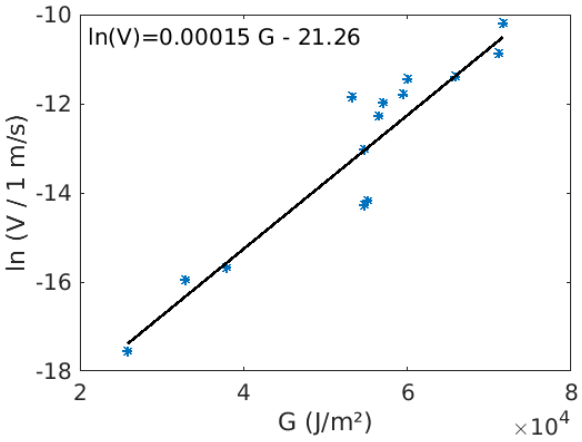

FIG. 20. Creep data in Ti-6A1-6V-2Sn titanium alloy in moist air, from Sastry et al.[19], figure 6a (beta annealed).

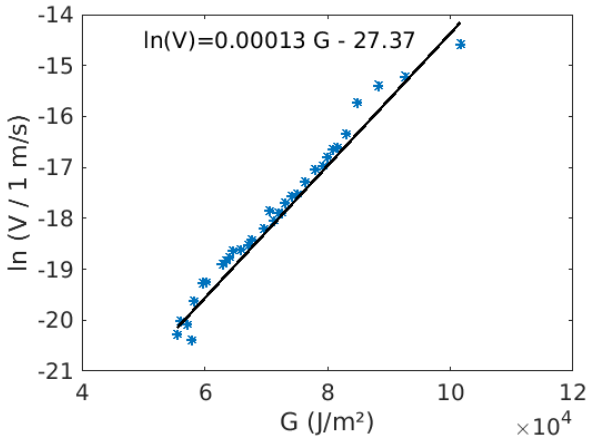

FIG. 21. Creep data of AISI 310S austenitic stainless steel in air, from Huang and Altstetter[20], figure 1 (uncharged plot).

[1] R. Toussaint, O. Lengliné, S. Santucci, T. Vincent-Dospital, M. Naert-Guillot, and K. J. Måløy. How cracks are hot and cool: a burning issue for paper. *Soft Matter*, 12:5563–5571, 2016. doi:10.1039/C6SM00615A.

[2] T. Vincent-Dospital, R. Toussaint, A. Cochard, K. J. Måløy, and E. G. Flekkøy. Thermal weakening of cracks and brittle-ductile transition of matter: A phase model. *Physical Review Materials*, 02 2020. doi: 10.1103/PhysRevMaterials.4.023604.

[3] S. M. Wiederhorn. Influence of water vapor on crack propagation in soda-lime glass. *Journal of the American Ceramic Society*, 50(8):407–414, 1967. doi: 10.1111/j.1151-2916.1967.tb15145.x.

[4] S.M. Wiederhorn and R.F. Jr. Krause. Crack growth in sapphire. In *Ceramic Engineering and Science Proceedings*, volume 23, pages 71–82. Wiley, 2002.

[5] P. M. Dove. Geochemical controls on the kinetics of quartz fracture at subcritical tensile stresses. *Journal of Geophysical Research: Solid Earth*, 100(B11):22349–22359, 1995. doi:10.1029/95JB02155.

[6] J. Holder, J. E. Olson, and Z. Philip. Experimental determination of subcritical crack growth parameters in sedimentary rock. *Geophysical Research Letters*, 28(4):599–602, 2001. doi:10.1029/2000GL011918.

[7] Y. Nara and K. Kaneko. Study of subcritical crack growth in andesite using the double torsion test. *International Journal of Rock Mechanics and Mining Sciences*, 42(4):521 – 530, 2005. ISSN 1365-1609. doi: 10.1016/j.ijrmms.2005.02.001.

[8] P.G. Meredith and B.K. Atkinson. Fracture toughness and subcritical crack growth during high-temperature tensile deformation of westerly granite and black gabbro. *Physics of the Earth and Planetary Interiors*, 39 (1):33 – 51, 1985. ISSN 0031-9201. doi:10.1016/0031-9201(85)90113-X.

[9] J. S. Nadeau. Subcritical crack growth in vitreous carbon at room temperature. *Journal of the American Ceramic Society*, 57(7):303–306, 1974. doi:10.1111/j.1151-2916.1974.tb10906.x.

[10] Y. Nara, M. Takada, D. Mori, H. Owada, T. Yoneda, and K. Kaneko. Subcritical crack growth and long-term strength in rock and cementitious material. *International Journal of Fracture*, 164(1):57–71, Jul 2010. ISSN 1573-2673. doi:10.1007/s10704-010-9455-z.

[11] W. Wang, T. Tong, and Q. Yu. Subcritical crack growth induced by stress corrosion in hardened cement paste. In *9th International Conference on Fracture Mechanics of Concrete and Concrete Structures*. FraMCos, 2016. doi: 10.21012/FC9.177.

[12] S. Santucci. *Croissance lente thermiquement activée et piégeage d'une fissure dans les matériaux structurés à une échelle mésoscopique : expériences et modèles*. PhD thesis, Ecole normale supérieure de Lyon, www.theses.fr/2004ENSL0288, 2004.

[13] A. G. Evans and S. M. Wiederhorn. Crack propagation and failure prediction in silicon nitride at elevated temperatures. *Journal of Materials Science*, 9(2):270–278, Feb 1974. ISSN 1573-4803. doi:10.1007/BF00550951.

[14] W. S. Oates, C. S. Lynch, D. C. Lupascu, A. B. K. Njiwa, E. Aulbach, and J. Rödel. Subcritical crack growth in lead zirconate titanate. *Journal of the American Ceramic Society*, 87(7):1362–1364, 2004. doi: 10.1111/j.1151-2916.2004.tb07736.x.

[15] J. Chevalier, C. Olagnon, and G. Fantozzi. Subcritical crack propagation in 3Y-TZP ceramics: Static and cyclic fatigue. *Journal of the American Ceramic Society*, 82(11):3129–3138, 1999. doi:10.1111/j.1151-2916.1999.tb02213.x.

[16] O. Lengliné, R. Toussaint, J. Schmittbuhl, J. E. Elkhoury, J. P. Ampuero, K. T. Tallakstad, S. Santucci, and K. J. Måløy. Average crack-front velocity during subcritical fracture propagation in a heterogeneous medium. *Phys. Rev. E*, 84:036104, Sep 2011. doi: 10.1103/PhysRevE.84.036104.

[17] M. Yoda, M. Nabetani, and W. Shim. Creep crack growth in polyethylene under combined mode I and mode II loading. *International Journal of Fracture*, 112(3):21–26, Dec 2001. ISSN 1573-2673. doi:10.1023/A:1022681718523.

[18] G. Hénaff, G. Odemer, and B. Journet. Creep and creep-fatigue crack growth in aluminium alloys. In *Aluminium Alloys, Theory and Applications*, pages 259–282. IntechOpen, 2011. doi:10.5772/15153.

[19] S. M. L. Sastry, R. J. Lederich, and B. B. Rath. Subcritical crack-growth under sustained load in Ti-6AI-6V-2Sn. *Metallurgical Transactions A*, 12(1):83–94, Jan 1981. ISSN 1543-1940. doi:10.1007/BF02648512.

[20] J. H. Huang and C. J. Altstetter. Internal hydrogen-induced subcritical crack growth in austenitic stainless steels. *Metallurgical Transactions A*, 22(11):2605–2618, Nov 1991. ISSN 1543-1940. doi:10.1007/BF02851354.